On the Feasibility of GPON Fiber Light Energy Harvesting for the Internet of Things

Article · January 2019

CITATION
1

READS
210

4 authors:

João Casaleiro
Instituto Politécnico de Lisboa
20 PUBLICATIONS **31** CITATIONS
SEE PROFILE

Carlos Carvalho
Instituto Politécnico de Lisboa
24 PUBLICATIONS **115** CITATIONS
SEE PROFILE

Pedro Viçoso Fazenda
Instituto Politécnico de Lisboa
10 PUBLICATIONS **78** CITATIONS
SEE PROFILE

Rui Policarpo Duarte
Technical University of Lisbon
39 PUBLICATIONS **104** CITATIONS
SEE PROFILE

i-ETC: ISEL Academic Journal of Electronics, Telecommunications and Computers
IoT-2018 Issue, Vol. 4, n. 1 (2018) ID-9

On the Feasibility of GPON Fiber Light Energy Harvesting for the Internet of Things

J. Casaleiro[a,b], C. Carvalho[a,b], P. Fazenda[a], R. P. Duarte[c,d]
[a] ADEETC, Instituto Superior de Engenharia de Lisboa (IPL-ISEL), CEDET, Lisboa, Portugal
[b] UNINOVA/CTS, Instituto de Desenvolvimento de Novas Tecnologias, Caparica, Portugal
[c] DEI, Instituto Superior Técnico (IST), Lisboa, Portugal
[d] INESC-ID, Lisboa, Portugal

jcasaleiro@deetc.isel.ipl.pt cfc@cedet.isel.ipl.pt pfazenda@cedet.isel.ipl.pt rpd@inesc-id.pt

Abstract **— The emerging concept of smart cities demands for a large number of electronic devices, like sensors and actuators, distributed over several public spaces and buildings. The Internet of Things (IoT) has a key role in connecting devices to the Internet. However, the significant number of devices makes the maintenance task of the entire network difficult and expensive. To mitigate this problem, considerable research efforts have been made to develop energy-aware devices capable of self-sustainable operation, by harvesting their energy from various sources. In this paper, we study the possibility of harvesting energy from the light flowing in the Gigabit Passive Optics Network (GPON) to supply low-power devices. Since most cities already have a working GPON installation, using this installation to interconnect and power IoT devices can be a viable and less expensive solution, instead of installing new dedicated networks. This is also an interesting solution to convey communications and energy to low-power applications where access to the power grid is unfeasible. This study is focused in the 1550 nm wavelength, whose available optical power, in residential premises, is between -7 dBm and +2 dBm. With this range of optical power, and with a 30% efficiency photodiode, we show, for the worst-case scenario of the GPON, how it is possible to harvest 62 µW of energy at the Maximum Power Point (MPP).**

Keywords: Energy harvesting, photodiode, optical fiber, GPON, IoT, wireless sensor networks, smart cities.

I. Introduction

Powering electronic devices using an optical fiber is a widely studied topic. The earliest work in this domain, which consisted on remote powering an alarm, was presented by Deloach et al. [1]. Since then, various power-over-fiber (PoF) systems have been proposed in the literature [2]-[21]. The development of devices capable of being powered from the same optical fiber they use for communications is a very challenging task. However, the motivation for addressing this challenge is sustained by several advantages. The power supply block that harvests energy from fiber is immune to all forms of electromagnetic interferences, short-circuits and electrostatic or atmospheric discharges [2]. Moreover, optical fibers also have low attenuation and are capable of working up to considerable distances, in excess of 20 km [3], thus constituting an interesting solution to be used in remote locations where power from the grid is not available.

The solutions that currently exist use optical sources with high power and dedicated fibers for powering purposes. Some PoF applications exist such as powering and reconfiguring remote nodes with and without batteries [5]-[6], powering optical splitters [7]-[8] and monitoring and signal measuring systems [9]-[10]. However, most of these applications make use of proprietary communication protocols that are not compatible with the existing telecommunication networks. This incompatibility makes it difficult, or even impedes, the establishment of low-cost sensor networks.

For smart city applications, where the implementation of large-scale sensor networks will be needed, the use of the GPON can be a viable and less expensive solution than installing dedicated networks. Most cities have installed GPONs that provide 2488 Mbps links for television, internet and telephone into residential buildings. The use of the existing networks for sensor interconnection has the advantage of simultaneously providing a communication channel and device powering, while avoiding the use of additional electric cables. The use of the latest generation networks to power sensors, as well as other devices, has been yet little explored [11]-[12]. Therefore, this paper presents a study on the possibility of using the light flowing in these networks, namely GPON, to supply energy to devices with low-power requirements.

In GPONs three communication bands are used: (1) the upstream band, with wavelengths between 1260 nm and 1360 nm, (2) the downstream band, between 1480 nm and 1500 nm, and (3) the RF video-overlay, between 1550 nm and 1560 nm. The latter band is used for broadcasting analog and digital television channels. This band is the most suitable for energy harvesting because the optical power, available in the 1550nm wavelength, ranges between -7 dBm and +2 dBm. Within this range, devices can extract between 60 µW and 475 µW.

This paper is organized as follows: Section II presents the state-of-the-art and discusses the existing PoF methods that are

currently used to power electronic devices, using optical fiber. Section III describes the methodology and the components that were used in the practical setup for measuring the amount of energy that can be harvested from the RF video-overlay band. Section IV presents the experimental results and a discussion on the feasibility of the proposed approach and Section V concludes this paper.

II. Background and Related Work

The use of optical fiber telecommunication networks with powering features began to be researched in the late 1990s. The powering of devices on the client side, e.g. telephone or modems, was the focus of that research. It was demonstrated that the application was not feasible because of the relatively big amount of power required by the equipment on the client side [6], [11], [17]. However, one must stress out that from this research it has resulted the testing of a system that provided the client with 0.5 W of power. A similar application for local optical fiber networks was presented by Miyakawa [18].

PoF is currently being used in remote sensor systems and power distribution networks [13]. Two different architectures are being used for optical power transmission: wavelength division multiplexing (WDM) and space division multiplexing (SDM). Some applications use the combination of both [3]-[4].

In SDM, depicted in Fig. 1 a), one or more fibers are used solely to power a device, while communication signals are allocated on another fibers [4]. Recently, for SDM, the use of double-clad fibers has been proposed to allow for the transmission of data in the core (in single mode) and the power in the second outer layer [14]-[15]. This architecture has the advantage of avoiding the need for using optical filters to split power and data, and interference between power and communications. The optical power transmitted is limited by the characteristics of the fiber. As an example, a SDM application is provided by Yasui et al. [16], where a system was developed to operate in high voltage environments, while providing 2 W continuously.

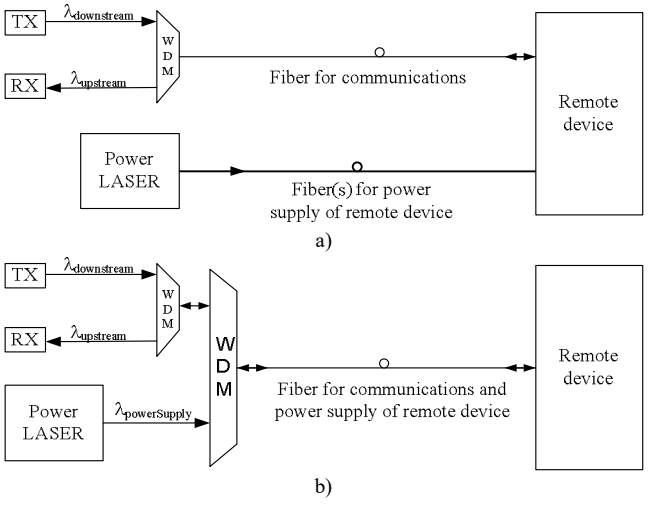

Fig. 1. a) SDM architecture and b) WDM for remote power supply.

In WDM, shown in b), the channels are separated into several different wavelengths over the same fiber. One of the wavelengths is used for powering purposes and, at least, two more wavelengths, for sending and receiving data. At the terminal devices, the various wavelengths are separated using dielectric filters and the optical energy from the energy carrier is converted into electrical energy, using a photodiode.

Comparing both architectures, WDM has the advantage of using only one fiber for both PoF and data. In the past, Peña et al. [19] showed how remote devices can be powered (extracting up to 205 mW) with WDM. In another application, Nango et al. [20] showed how to power remote sensor nodes for measurements of the electric field radiated in anechoic cameras. Nevertheless, PoF applications over the GPON are severely limited by the energy optimization of the network [21] and mainly by the characteristics of the single mode fibers being used [4]. In particular, the nonlinearities existing in this kind of fiber, such as the Brillouin and Raman scattering, introduce a low return loss, limiting the maximum power in single mode fibers to 20 dBm. The safety limits for laser emission into the fiber are defined in the IEC/EN 60825 standard and the maximum allowed levels are about hundreds of milliwatts, so as not to render the fiber inoperable because of micro curves [4], [6], [17].

The IoT research domain has been focusing on energy harvesting solutions based on the light [22], Radio Frequency (RF), and vibrations [23]-[25]. The use of the energy coming from the normal operation of the fiber has not drawn too much attention [26]. The main reason is because the optical power in data transmission, using wavelengths ranging from 1310 nm to 1490 nm, is quite small, -30 dBm. However, as it was already said, the power of the RF video-overlay service, in the 1550 nm wavelength, is substantially higher (-7 dBm to +2 dBm). Moreover, since this is a unidirectional service, the service provider cannot alter or adjust the power as a function of the number of clients using this service. Therefore, this opens a novel PoF opportunity for low-power IoT applications.

III. Description of the IoT Node Blocks

The IoT node proposed in this paper consists of a harvester, a power management unit (PMU), an energy storage device and a load, as shown on the right-hand side of Fig. 2. To harvest the energy from the fiber optics network, a PIN photodiode is used. The energy obtained by the harvester can be stored, or it can be transferred directly to the load. The storage uses a capacitor sized for the specific energy requirements of the application. As a proof of concept, a microcontroller and a LED are used as a load.

One assumes that the node will work in a duty-cycling mode, meaning that the device has an active period, T_{ON}, and an idle period, T_{OFF}, as shown in Fig. 3.

The operation duty-cycle is given by

$$\delta = \frac{T_{ON}}{T_{ON} + T_{OFF}} = \frac{T_{ON}}{T}. \quad (1)$$

Using a simplified energy balance approach, one can design the storage capacitance needed for a specific application.

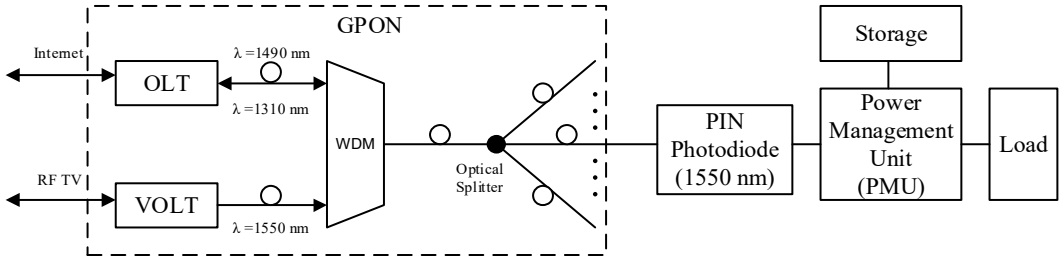

Fig. 2. Schematic illustration of the GPON (on the left) with the Optical Line Terminal (OLT) and the RF video-overlay OLT (VOLT) combined with a wavelength division multiplexer (WDM) and an optical splitter. On the right-hand side is the system block diagram of the IoT node with the harvester (PIN photodiode), PMU, storage and the load.

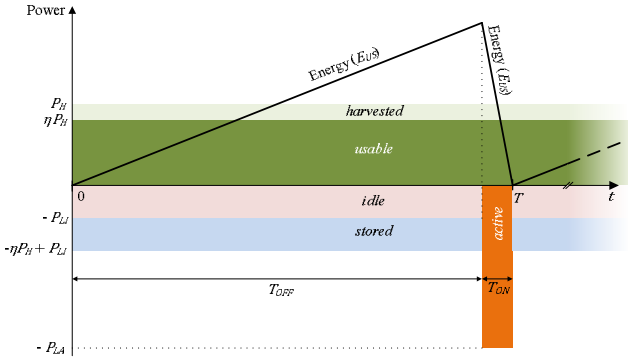

Fig. 3. Power and energy budget for duty-cycling mode.

Thus, if the incident power and the temperature are constant, the energy supplied by the harvester can be described as

$$E_H = \int_0^T P_H \, dt = P_H \times T, \tag{2}$$

where P_H is the instantaneous output power of the harvester and T is the cycling period.

Regarding the load power supply, two energy levels must be considered. When active, the energy required by the load is given by

$$E_{LA} = \int_{T_{ON}} P_{LA} \, dt = P_{LA} \times T_{ON}, \tag{3}$$

where P_{LA} is the instantaneous load power when active. When the load is idle, its energy consumption is given by

$$E_{LI} = \int_{T_{OFF}} P_{LI} \, dt = P_{LI} T_{OFF} = P_{LI}(T - T_{ON}), \tag{4}$$

where P_{LI} is the instantaneous load power when idle.

Considering a capacitor as the storage element, the energy it can accumulate is given by

$$E_S = \frac{1}{2} C V_C^2, \tag{5}$$

where C is the storage capacitance and V_C is the voltage level of the storage element. It should be noted that the node cannot consume all the stored energy, because a minimum voltage, V_{Cmin}, is required to supply the PMU. Thus, the usable energy in each cycle is given by

$$E_{US} = \frac{1}{2} C (V_{Cmax}^2 - V_{Cmin}^2), \tag{6}$$

where V_{Cmax} is the threshold voltage level to protect the storage element from overcharging. This threshold can be configured in the PMU.

To obtain a self-sustainable node, the following criteria are required:

$$\begin{cases} \eta \cdot \delta \cdot E_H + E_{US} \geq E_{LA}, & \text{when active} \quad (7a) \\ \eta \cdot (1-\delta) \cdot E_H \geq E_{LI} + E_{US}, & \text{when idle} \quad (7b) \end{cases},$$

where η is the efficiency of the PMU.

Substituting (1), (2), (3) and (4) into (7) and assuming that all the stored energy will be delivered to the load, results in

$$\begin{cases} \eta P_H T_{ON} + E_{US} = P_{LA} T_{ON}, & \text{when active} \quad (8a) \\ \eta P_H (T - T_{ON}) = P_{LI}(T - T_{ON}) + E_{US}, & \text{when idle} \quad (8b) \end{cases}.$$

Solving (8a) to E_{US} results in

$$E_{US} = (P_{LA} - \eta P_H) T_{ON}. \tag{9}$$

Substituting (6) into (9) and solving to C, one obtains the minimum capacitance for the storage element, given by

$$C = \frac{2(P_{LA} - \eta P_H) T_{ON}}{V_{Cmax}^2 - V_{Cmin}^2}. \tag{10}$$

Adding (8a) to (8b) gives

$$\eta P_H T = P_{LA} T_{ON} + P_{LI}(T - T_{ON}), \tag{11}$$

from which the duty-cycle is obtained:

$$\delta = \frac{\eta P_H - P_{LI}}{P_{LA} - P_{LI}}. \tag{12}$$

It is clear from (12) that the usable power ηP_H must be larger than the idle load power, i.e. $\eta P_H > P_{LI}$ for the system to be self-sustainable.

A. Harvester characterization and modeling

The photodiode is used in photovoltaic (PV) mode, working as a PV cell. In this mode, the photodiode generates a current (photocurrent) proportional to the incident light power that it receives in its active area. The equivalent electrical model of a PV cell consists of a light-induced current source (I_l), in parallel with a diode D (acting as a voltage limiter), a shunt resistance (R_p) and a series resistance (R_s), as shown in Fig. 4.

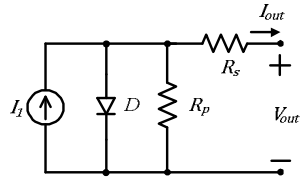

Fig. 4. Equivalent electrical model of a PV cell.

The series resistance is due to the resistance of the metal contacts, ohmic losses in the front surface of the cell, impurity concentrations, and junction depth. From the electrical model (Fig. 4), the output current (I_{out}) is given by

$$I_{out} = \left(\frac{R_p}{R_p+R_s}\right)\left[I_1 - I_S\left(e^{q\frac{v_{out}+R_S i_{out}}{nkT}} - 1\right) - \frac{V_{out}}{R_p}\right], \quad (13)$$

where I_S is the limit of the current in the diode under high reverse bias, q is the electron elementary charge ($1.60217657 \times 10^{-19}$ C), k is the Boltzmann constant ($1.380648813 \times 10^{-23}$ J/K), T is the ambient temperature, expressed in Kelvin, and n is the emission (or ideality) coefficient, which equals 1 for an ideal diode. Moreover, if the diode did not exhibit breakdown, the maximum reverse current that one could get through the diode, with an infinite reverse bias, would be I_S. Another definition for it, is that it is the "dark saturation current", i.e. the diode leakage current density in the absence of light.

Measurements were obtained using the fiber triplexer ITR-D3T-SD6-2 from the Source Photonics manufacturer. Using a triplexer has the advantage of having WDM that separates light for device powering (in the 1550 nm wavelength) and light for the data, as shown in Fig. 5.

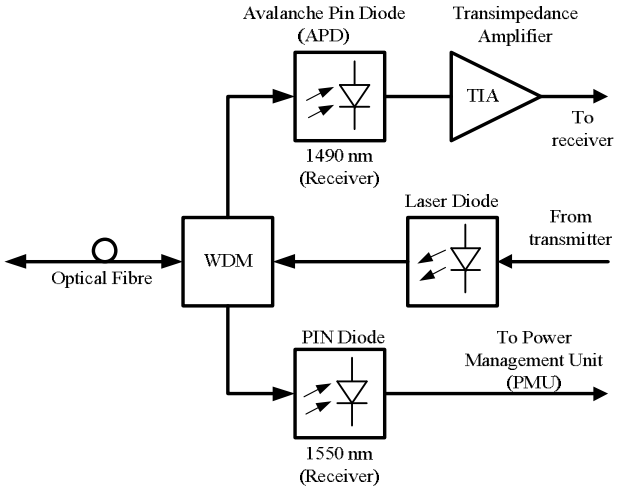

Fig. 5. Internal block diagram of the optical fiber triplexer ITR-D3T-SD6-2, from the Source Photonics manufacturer.

The PIN diode of the triplexer is usually used to demodulate the RF video-overlay signal and was not specifically designed for energy harvesting purposes as a PV cell is. Thus, this photodiode needs to be studied for this kind of assignment. As such, to assess the power that can be harvested from the GPON, the PIN photodiode was characterized, for several optical power levels.

By measuring the output voltage and current of the PIN photodiode for several load values, we obtained its I-V characteristics, which is shown in Fig. 6. The PIN photodiode characteristics were obtained for distinct optical power levels, measured using a JDSU OLP-35 optical power meter.

From Fig. 6, the open circuit voltage of the harvester can be obtained. This is an important parameter because it sets the minimum cold start voltage of the PMU.

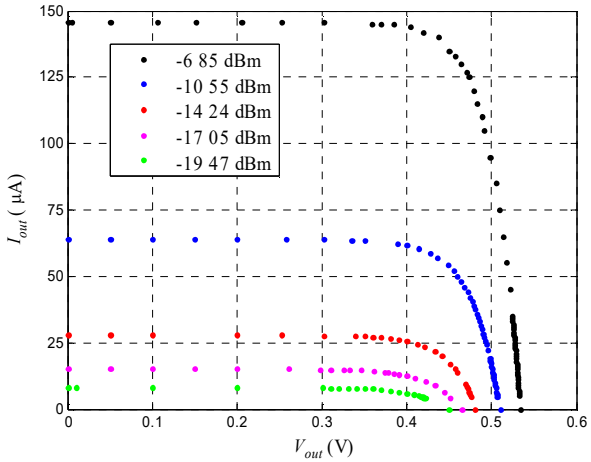

Fig. 6. Photodiode I-V characteristic measured values for various incident optical power values.

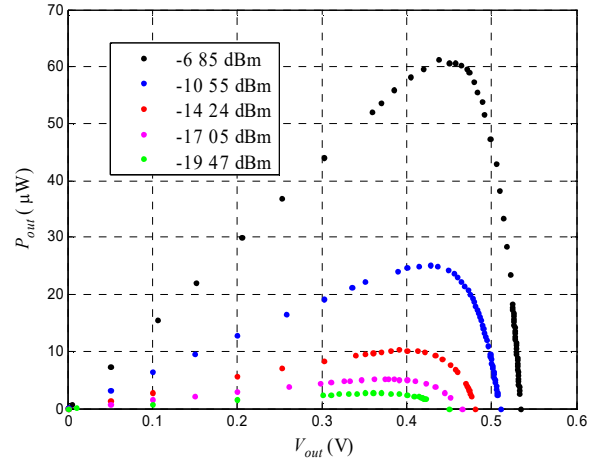

Fig. 7. Photodiode P-V characteristic for various incident optical power values.

From the I-V characteristics it is possible to obtain the P-V characteristics, shown in Fig. 7, which are important to determine the Maximum Power Point (MPP). Fig. 7 shows the output power ($P_{out} = I_{out} \times V_{out}$) extracted from the harvester as a function of the output voltage.

By looking into Fig. 7, one can inspect which is the ratio between the voltage of the MPP and the open circuit voltage (V_{OC}). This ratio (k), for each incident optical power, is computed and documented in TABLE I.

TABLE I
RATIO BETWEEN V_{MPP} and V_{oc}

Optical input power P_{in} (dBm)	Open circuit voltage V_{oc} (V)	MPP voltage V_{MPP} (V)	Ratio $k = V_{MPP}/V_{oc}$ (%)
-6.85	0.535	0.438	81.78
-10.55	0.512	0.429	83.77
-14.24	0.481	0.400	83.29
-17.05	0.466	0.374	80.37
-19.47	0.450	0.360	80.00

The value of the k ratio agrees with the ones commonly known in the literature, for example, in [27].

Through the analysis of Fig. 6 and Fig. 7, it is possible to extract some simple data concerning the performance of the photodiode. This information is summarized in TABLE II. An important parameter is the conversion efficiency of the harvester (η_E), which is defined as the ratio between the maximum power output of the harvester, i.e. the power at the MPP, and the optical incident power, shown at the rightmost column of TABLE II.

TABLE II
MEASURED CHARACTERISTICS FROM THE PHOTODIODE

Optical incident power P_{in} (dBm)	Short circuit current I_{sc} (μA)	Open circuit voltage V_{oc} (V)	Maximum output power P_{max} (μW)	Efficiency at the MPP η_E $\eta_E = P_{max}/P_{in(\mu W)}$ (%)
-6.85	146	0.535	62	30.0
-10.55	64	0.512	25	28.4
-14.24	28	0.481	10	26.5
-17.05	15	0.466	6	30.4
-19.47	8	0.450	3	26.6

It is worth to note that

$$P_{in(\mathrm{dBm})} = 10\log_{10}\left[P_{in(\mu W)}\right] - 30 \tag{14}$$

and that

$$P_{in(\mu\mathrm{W})} = 10^{\frac{P_{in(\mathrm{dBm})+30}{10}}}. \tag{15}$$

By analyzing the data plotted in Fig. 6, along with the electrical equivalent depicted in Fig. 4, one can extrapolate the values of the parameters in the model, namely, I_1, I_S, n, R_s and R_p. Obtaining the value of these parameters is useful to simulate the behavior of the photodiode in an electrical simulation computer program.

There are essentially two ways to extract the parameter's values. One is solving a system of algebraic transcendental equations, and a comprehensive survey about it can be found in [28]. The other way is to use optimization algorithms that determine the parameters numerically. The least mean squares method is the most popular. The parameters are calculated by minimizing the error between the measured data and the theoretical curve and beforehand, each of the parameters to be obtained is bounded by a lower and an upper value, considered to be consistent with the order of magnitude of the true parameter. The photodiode parameters were extracted using the MATLAB® function `lsqnonlin()` with a tolerance of 10^{-12} and a maximum number of iterations of 1000. This function solves nonlinear least squares curve fitting problems numerically. For each of the light intensities that were tested, the extraction of the five parameters that make up the model, have the results listed in TABLE III.

In order to confirm that the extracted values are the correct ones, the photodiode output current function (I_{out}), shown in equation (13), is plotted using the values of TABLE III and checked against the measured data of Fig. 6, in order to verify if they match. The resulting plots are shown in Fig. 8.

TABLE III
PHOTODIODE EXTRACTED PARAMETERS FOR THE ELECTRICAL MODEL

Incident Power (dBm)	I_1 (μA)	I_s (pA)	n	R_s (Ω)	R_p (MΩ)
-6.85	146.5	6.18	1.224	29.6	9.52
-10.55	63.9	7.43	1.243	20.7	10.0
-14.24	27.8	5.55	1.216	0.0	3.62
-17.05	15.1	37.07	1.401	100.0	10.0
-19.47	8.1	41.44	1.435	100.0	10.0

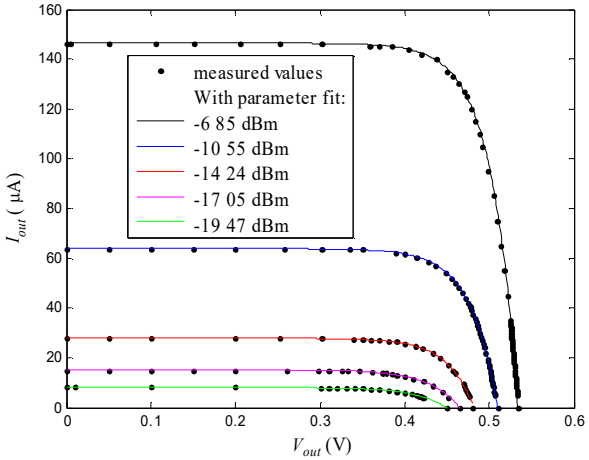

Fig. 8. Photodiode I-V characteristic with measured data (dots) and analytical function using extracted parameters (lines).

By observing Fig. 8, one can confirm that there is a close match between the set of dots obtained by experimental measurements, and the theoretical function using the extracted parameters.

Moreover, by using the values of the obtained parameters into the electrical model of Fig. 4, and using the LTspice® electric circuit simulator, a simulation was now run for each value of incident optical power. The resulting plots are shown in Fig. 9, where they are compared with the ones already shown in Fig. 8.

Given the functions depicted in Fig. 9, it can be noted that there is also a very strong match between the analytical curves and the ones obtained by the computer simulation of the electrical model.

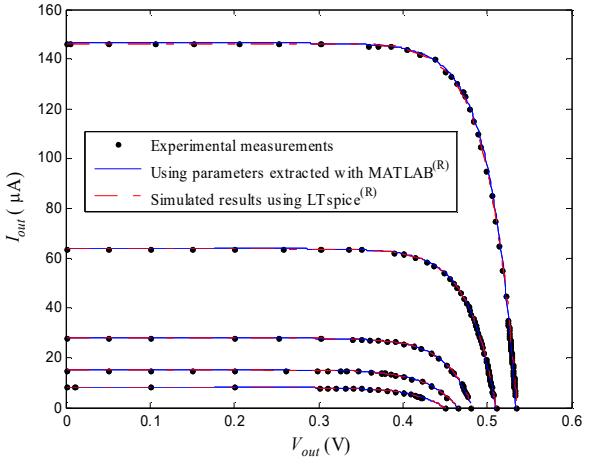

Fig. 9. Photodiode I-V characteristics using analytical functions with extracted parameters (blue) and electrical simulation results (dashed red).

Although at naked eye, the electrical model function (13), as well as its electrical simulation, are very close to the original measured values, it is important to quantify how close they are. As such, the plot of the relative error is shown next, in Fig. 10 and Fig. 11, for the analytical and the simulated functions, respectively.

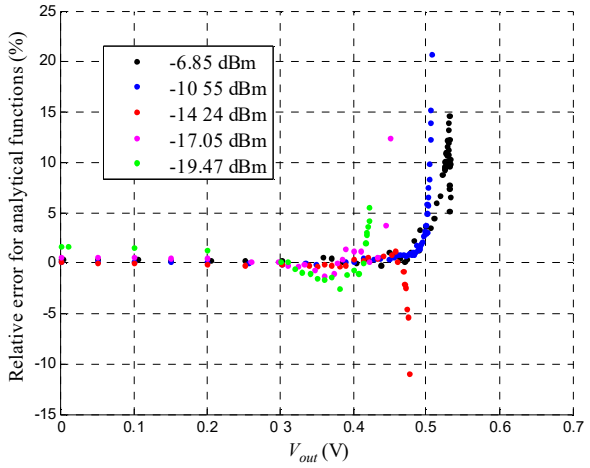

Fig. 10. Relative error between the experimental currents and the ones obtained by the analytical functions with extracted parameters.

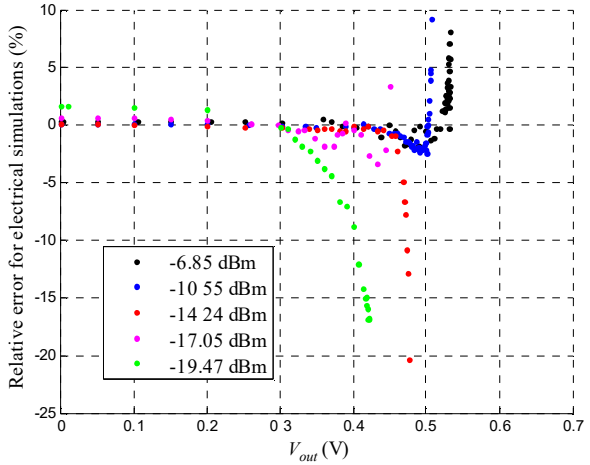

Fig. 11. Relative error between the experimental currents and the ones obtained by electrical simulation of the extracted model.

By inspecting both Fig. 10 and Fig. 11, a common pattern can be identified for each input power, in which the relative error increases with V_{out}, especially when it approaches the value of the open circuit voltage. This is because when the derived function, either the analytical or the electrical simulated one, is in its steepest zone, there is a progressive increase in the deviation from the original values. This deviation is more critical as one gets closer to the open circuit voltage. Nevertheless, at the MPP (see TABLE I), for each of the input levels, the relative error is below 3%. In addition, for the most unfavorable value of the relative error, the absolute current error is less than 1 µA. Given that the GPON operates between -7 dBm and +2 dBm, the most meaningful input power values are those at higher levels of optical power. Thus, the most representative function is the one at -6.85 dBm, where the relative error tends to be smaller than for the other optical levels in the same variation zone.

B. Power Management Unit

The function of the PMU is to process the energy harvested by the photodiode, stepping it up and sending it to the storage element, or directly to the load, if the storage is already full.

The selection criteria to be fulfilled must encompass a step-up DC-DC converter capable of working with very low voltages, below 0.5V. The V_{oc} of the photodiode is in the range of 0.4 V to 0.6V. Thus, a DC-DC step-up converter, with the capability of having a cold start input voltage below the lower bound of this range, must be selected. If the demand for this worst case is met, the PMU will always start.

Thus, such a converter was selected, consisting in the ADP5091, provided by Analog Devices®. This integrated circuit was chosen because of its functional characteristics and for being a relatively recent device in the market. The cold start operating input voltage of the ADP5091 is 380 mV [29]. This PMU has an evaluation board whose features were sufficient and suited, on one hand, to have the voltage coming from the photodiode stepped-up, and on the other hand, to have a supercapacitor being charged with the energy harvested from the photodiode. The abovementioned board is shown in Fig. 12.

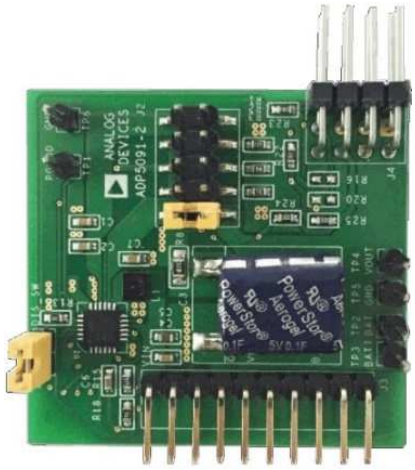

Fig. 12. Photograph of the ADP5091-2-EVALZ evaluation board [30].

This board encompasses a ADP5091 PMU, a storage supercapacitor, and additional circuitry (resistors, mainly) to configure key voltage levels. This PMU can charge storage elements such as rechargeable batteries, supercapacitors, or even conventional capacitors.

The ADP5091 PMU performs Maximum Power Point Tracking (MPPT), which keeps the input voltage ripple in a fixed range near the MPP of the harvester. The purpose is to make the harvesting process as efficient as possible. Moreover, it has sensing modes with programming regulation points of the input voltage, which allow for the extraction of the highest possible energy from the harvester. A programmable minimum operation threshold enables shutdown during a low input condition. A typical operation circuit, taken from the manufacturer datasheet [29], is shown in Fig. 13.

The adopted settings for the proposed approach mainly make use of the TERM pin (bottom right-hand side of Fig. 13), whose function is to set the value up to which the supercapacitor will charge (V_{Cmax}, previously defined). Using the default settings of the board, this voltage is preset to 3.5 V.

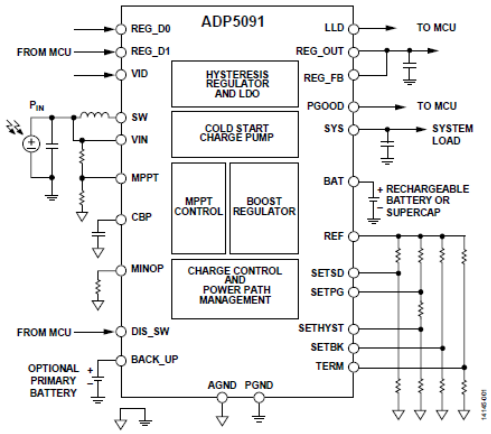

Fig. 13. Typical application circuit [29].

To perform the MPPT, and based upon the data gathered in TABLE I, the value of k that was chosen to work with the DC-DC converter is 82%. This value can be set by establishing a voltage divider over the input voltage. One can check in Fig. 13 that, at the left-hand side, between the VIN terminal and the ground terminal, there is a voltage divider, yielding a voltage to the MPPT pin. The ratio of this voltage divider is the one that needs to be set, to have $k \approx 0.82$ (see TABLE I). Thus, the pull-down resistor (R_{18} in [30]) is set to 18 MΩ, keeping the default value used the evaluation board. However, value of the pull-up resistor (R_{15}) needed to be adjusted to 3.9 MΩ, leading to a change in the original value used by the board, so that the value experimentally determined for k could be met. In fact, when wiring together the photodiode and the board, and using the original supercapacitor shipped with it (0.1 F), it takes 8h47m to fully charge it to 3.5 V. If the original setup was used instead (with $R_{15} = 4.7$ MΩ), it would take 9h11m to achieve the same goal. Thus, it takes 24 minutes more, as the MPP is deviated from the optimum point, confirming the importance of setting the MPPT voltage divider to the value determined in TABLE I.

Even though the board itself is fitted with a 0.1 F supercapacitor, this capacitor was replaced by several other capacitors with higher values, to store more energy and study the charging curve over an extended period of time.

C. Storage device

The harvested energy is stored in a supercapacitor. This device has the purpose of storing energy using a double layer between an electrolyte and a solid, in which the inner structure is composed by two electrodes immersed into an electrolyte, which can be liquid or solid, and that are separated by a membrane. These capacitors differ from rechargeable batteries because they store energy at the surface of the electrodes, unlike batteries, that store energy thanks to an electrochemical reaction. Because of this, supercapacitors can stand a higher number of charge and discharge cycles than batteries can, being suited for applications where this kind of regime is usual. The number of these cycles can be as high as a million, leading to an operational lifetime of ten years, until the capacitance value starts to show some signs of degradation [31], because of the degradation of the electrodes and of the electrolyte solution. One very appealing factor about supercapacitors is that they do not require specific charging circuits, being able to stand trickle charging.

Supercapacitors are inexpensive, making them very appealing to use in opposition to rechargeable batteries, as these are more expensive. Examples of systems that are designed to make use of a supercapacitor to store harvested light energy can be found in [32]-[33]. There are also some applications that use both a battery and a supercapacitor [34]. These act as primary and secondary energy storage, respectively.

With rechargeable batteries, there are only a few typical voltage ratings, depending on the technology being used. With supercapacitors, these ratings are much more diverse, similarly to regular capacitors. This factor is also important, not only because of the end application, but also because it can result in a smaller device, if a lower voltage rating is allowed. Fig. 14 shows the supercapacitors that were selected to be used in the experiments with the energy harvesting application in this work, all of them having a rating of 5 V.

Fig. 14. Supercapacitors selected for the application (5 F, 3 F, 1 F and 0.1 F).

It must be considered that, for typical low-power energy harvesting applications, the size of the whole system is intended to be small. As such, although the capacitance value, for supercapacitors, can reach values as high as 3000 F, for practical small sized applications, due to body size restrictions, the selected supercapacitors must have lower values, as well as their voltage rating.

The higher the capacitance value, the larger will be the leakage current due to self-discharge. Moreover, the leakage current increases in proportion to the increase in the voltage at the terminals of the supercapacitor. The leakage current can be modeled as a resistor placed in parallel with the capacitor. According to the manufacturer's datasheet [35]-[36], the leakage current for each capacitor in Fig. 14 is presented in TABLE IV.

TABLE IV
LEAKAGE CURRENT FOR THE SUPERCAPACITORS THAT WERE USED

Capacitance (F)	Leakage current @20ºC and @5.0V (μA)
0.1	3
1.0	12
3.0	16
5.0	25

IV. EXPERIMENTAL RESULTS

Some experimental results have been determined so far, given that the photodiode was characterized from an experimental point of view. From the set of measurements, by varying the output conditions of the photodiode from short

circuit to open circuit, it was possible to obtain the various values of current that, subsequently, allowed for obtaining the data in TABLE I, TABLE II and TABLE III.

The measurements setup is shown in Fig. 15, which includes one oscilloscope (Tektronics TDS 2004B) and two digital multimeters (Agilent Keysight 34401A). The laser was generated using a JDSU (OLS-38), at the wavelength of 1550 nm and a power of -7 dBm.

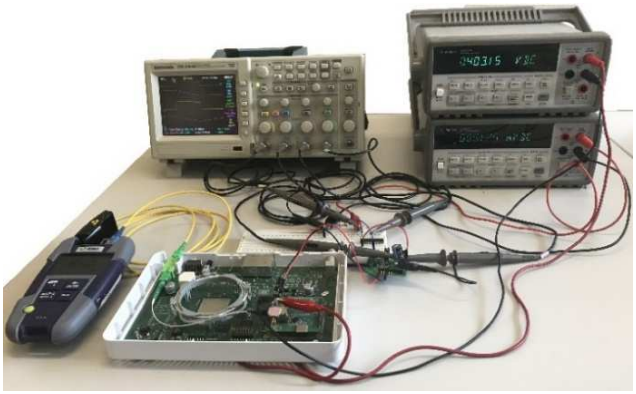

Fig. 15. Photo of the measurements setup.

A. Performance of the supercapacitors

Several tests have been run to determine how long would it take to charge a supercapacitor of a given value, connected to the BAT pin of the DC-DC converter, from a 0 V condition (cold start). Just as described in section III.B, the terminal voltage of the charging process is set to 3.5 V. For each of the devices shown in Fig. 14, the results of their charge, using an optical incident power of -6.85 dBm, at the wavelength of 1550 nm, have been recorded. The voltage variation at terminals of the supercapacitor (V_C) is shown for each unit. The horizontal axis is normalized to hours per Farad, so that all the voltages representing the charge can be compared on a common basis.

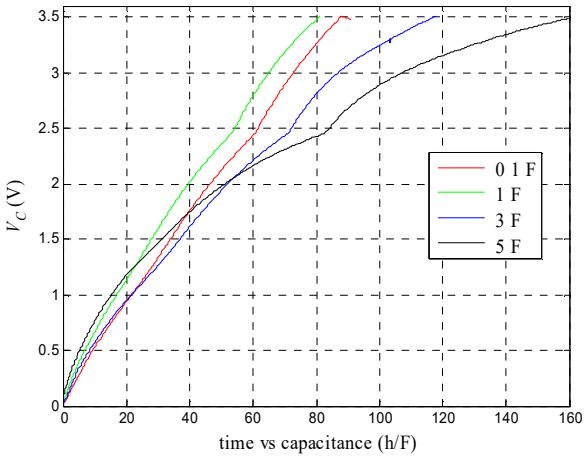

Fig. 16. Normalized voltage variation (during charge) of the supercapacitors.

The time needed to charge each of the supercapacitors up to 3.5 V (starting from zero), is indicated in TABLE V, as well as their stored energy. From Fig. 16, one can conclude that the supercapacitor that has the highest rate of charge per unit of capacitance is the one with 1 F.

TABLE V
CHARGING DATA FOR EACH SUPERCAPACITOR

Capacitance (F)	Time of charge to 3.5 V (days hours minutes)	Stored energy (J)
0.1	00d 08h 47m	0.6125
1.0	03d 09h 10m	6.1250
3.0	14d 16h 09m	18.375
5.0	33d 16h 18m	30.625

Although, in principle, this does not agree with the data in TABLE IV, it is to note that both the temperature and the working voltage that were used are not the same as in the datasheet, nor constant. Moreover, when referring to the source of input power to the circuit (the photodiode), one must bear in mind that temperature is a variable to consider for the current generation. For those longer periods of time to get the supercapacitor fully charged, the temperature variation is bigger, given that it spans for a full 24-hour cycle, for several days. Also, a common remark for any of the capacitances reported in Fig. 16, is that when the voltage reaches slightly less than 2.5 V, the charging regime suffers a change. This change is directly associated with the mode of operation of the DC-DC converter, when it enters synchronous mode [29] and the output voltage is driven to follow the voltage of the storage device.

B. Powering an electronic application

As described in the datasheet of the ADP5091, the average value for the efficiency of the DC-DC converter is about 80% (assuming its worst-case scenario). To check if the approach tried in this paper is feasible, a simple electronic application was built. The power supply is obtained from the PMU to demonstrate that it is possible to harvest energy from the GPON, store it, and use it to supply a low power IoT sensor node. The application consists of a PIC16F1459 Micro Controller Unit (MCU), running a program that periodically turns a LED on and off using a very low duty-cycle. The timings where calculated so that this application, after starting up, could permanently remain in operation. During the interval of time when the LED stays turned off, the MCU remains turned on, in a sleeping mode, maintaining the internal oscillator running and the watchdog timer to periodically wake up. A picture of this application, being powered by the PMU, is shown in Fig. 17.

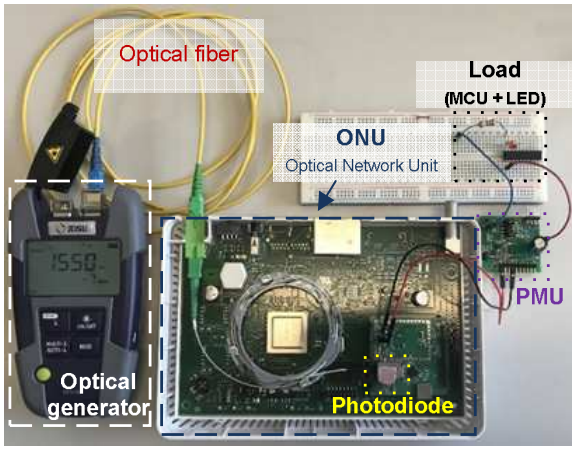

Fig. 17. Electronic application: powering a MCU that flashes a LED.

The optical generator provides a laser with an incident power of approximately -7 dBm (actually, -6.85 dBm), which is converted to electrical power by the photodiode and is delivered to the PMU that manages the charge of a capacitor and the power supply for the application.

In Fig. 18, it is shown a cold start of the PMU, where it can be identified the various stages that the supplying voltage goes through until it starts powering up the MCU.

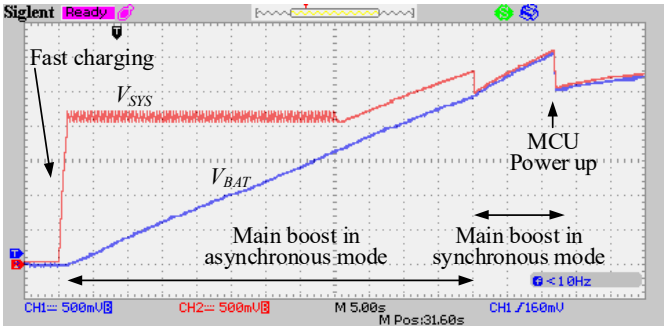

Fig. 18. Phases of operation, from cold start until the MCU (load) powers up.

As it can be seen Fig. 18, this takes about 72 s. Note that when VBAT reaches about 2.5 V, i.e. about 60 s after the cold start, the DC-DC converter enters the synchronous mode, as already mentioned. VBAT is the name adopted by the datasheet of the ADP5091 to identify the voltage of the storage device. However, this voltage has been introduced before in this paper and is named V_C. V_{SYS} is the output voltage of the PMU, which directly interfaces with the load to supply it.

The ADP5091 is configured to swing the charging and discharging voltages of the storage element between $V_{Cmax} = 3.2$ V and $V_{Cmin} = 2.5$ V, respectively. Let us consider the scenario where the load, when active, requires $P_{LA} = 2.5$ mW during $T_{ON} = 211$ ms and $P_{LI} = 35.5$ µW, when idle. According to (10) and (12), the value of the storage capacitance will be $C = 259$ µF and the duty-cycle $\delta \approx 0.5\%$. Using the E6 series, the nearest capacitance value is 330 µF. The cycling period is $T = T_{ON} / \delta = 42.2$ s.

Since the capacitor is small, when there is a demand for energy, it rapidly drains out. This is the reason why there is a drop in the value of V_{SYS} and V_{BAT} when the MCU is turned on, because the first thing it does is to turn the LED on, thus demanding a reasonable amount of current.

The current consumption when the MCU is in sleep mode is 12.5 µA, as measured using a digital ammeter. When the MCU wakes up, it turns the LED on for approximately 211 ms increasing the supply current to 880 µA. In addition, it can also be noted that the decreasing variation in V_{BAT} is approximately 500 mV, as shown in Fig. 19. To have a broader perspective about how the voltages in Fig. 19 evolve over time, one can observe Fig. 20.

From the above results we conclude that the minimum usable power that can be extracted from a GPON is 48 µW, for -7 dBm (200 µW) of optical power, assuming an efficiency of 30% for the photodiode and 80% for the DC-DC converter.

If a more power demanding application is to be supplied, a longer interval must be allowed for the storage device to charge, in addition to having a device with a higher storage capacity. If the purpose is to supply a ONT module for data transmission, encompassing the phases that go from powering up the module, obtaining the IP address and then communicating the intended data, enough energy must be harvested.

After the characterization of the various supercapacitors, it is possible to estimate the energy needed to power a GPON Small Form-factor Pluggable Optical Network Terminal (GPON-SFP-ONT). These have a lower power consumption when compared to the power that other ONTs put available to customers through service providers.

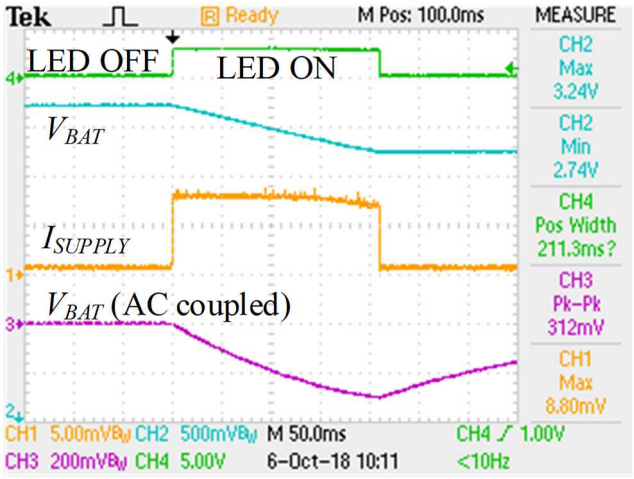

Fig. 19. Detail showing the current consumption and related waveforms.

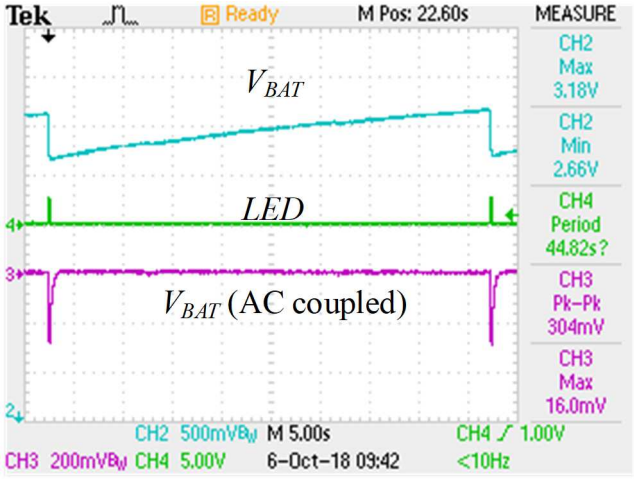

Fig. 20. Variation of the working voltages during long term operation.

In TABLE VI, the consumption of some GPON-SFP-ONT modules is shown, to serve as a guide to size the features of the supplying system.

TABLE VI
SFP GPON-ONT MODULES

Manufacturer / Model	Current [mA]	Power [W]
Finisar FTGN2117P2xxN	450	1.418
WTD RTXM167-522	200	0.627
MicroTik FG1537TWGPA04T8	600	1.884
Prolabs GPON-SFP-OLT-B+-NC	500	1.565
Delta Electronics OPGP-34-A4B3SL-B	400	1.252

Let us consider the use of the less power hungry GPON-SFP-ONT in TABLE VI, the WTD RTXM167-522 [37], which has a bit rate of 2488 Mbps for upstream and 1244 Mbps on downstream. If this device is used for 10 seconds, to periodically transmit data collected over a relatively long period (e.g. billing telemetry), system sizing can be carried out as follows. For the same voltage swing in V_{BAT} (V_C) as before, if a constant power of 627 mW and an ON time of 10 s is considered, according to equations (10) and (12), the value of the storage capacitance is $C = 3.2$ F and the duty-cycle is $\delta \approx 19.94\times10^{-6}$, i.e $T = 5.8$ days. Note that this result does not take into consideration the leakage current of the storage device, which increases with larger capacitance values. For a capacitance of 3 F, the leakage current cannot be neglected, as shown in Fig. 16 and TABLE IV. Moreover, considering the leakage and temperature variation, one obtains (from Fig. 16) a charging time of 3.17 days, i.e. 3 days and 4 hours. However, note that the charging times in Fig. 16 are taken with no load, i.e. $P_{LI} = 0$ µW, which explains the shorter charging time, compared to theoretical expected results.

V. Conclusions

This paper presented a feasibility study about harvesting light energy flowing in GPON, store it, and use it to supply low-power nodes for the IoT. The harvested light comes from the RF video-overlay wavelength in 1550 nm. The instantaneous energy extracted from the fiber is small and, in the worst case, it is 60 µW. Storing it into a supercapacitor over time, allows for periodically powering an application with more demanding requirements.

Experimental results show that it is possible to power low-power nodes from a GPON with low duty-cycle activity and extremely low power when devices are in idle or sleeping. In the worst case, it should be less than 48 µW. The theory was validated by a prototype that periodically powers a 2.5 mW load during 211 ms, with a period of about 44.8 seconds. With an incident power of -6.85 dBm, the present study can serve as a worst-case scenario that can be obtained from the GPON.

A theoretical scenario to power a GPON ONU with a 627 mW during 10 seconds with a periodicity of 6 days was presented. Theory shows that it is possible to power a IoT node from the GPON and use the GPON to send the collected data to a remote server.

A design framework was derived, so that the designer can conveniently determine both the values of the storage capacitance and the operating duty-cycle. In the approach that was followed, a working methodology was also established to characterize the harvester photodiode using a numerical least squares approach and establish its electrical model. In addition, several supercapacitors were studied, by letting them charge over a large period, encompassing several days, as it would happen in a real low duty-cycle situation. From this study, the effects of the leakage current were observed. A commercial PMU was selected, to manage the charging process of the storage device and to serve as the power supply to the load. The circuitry around the PMU was configured to be in accordance to the MPP of the harvester, thus enabling MPPT.

Acknowledgements

The authors wish to thank to Fábio Martinho and Rui Lopes for the measurements of the supercapacitors charging voltages. Also, the authors wish to thank to Sérgio André for his helpful work in disassembling the optical module and for several helpful discussions about this work.

References

[1] B.C. Deloach, R.C. Miller and S. Kaufman. Sound alerter powered over an optical fiber. Bell Syst. Tech. Journal, Vol. 57, pp. 3303-3316, 1978

[2] A. Basanskaya. Electricity over Glass [fiber optic to transfer electric power]. IEEE Spectrum, Vol. 42, No. 10, pp. 18, 2005.

[3] M. Dumke, et. al. Power Transmission by Optical Fibers for Component Inherent Communication. Journal of Systemics, Cybernetics and Informatics, Vol. 8, No.1, pp. 55-60, 2010.

[4] T. C. Banwell, R. C. Estes, L. A. Reith, P. W. Shumate and E. M. Vogel, Powering the fiber loop optically-a cost analysis. Journal of Lightwave Technology, Vol. 11, No. 3, pp. 481-494, March 1993.

[5] J.G. Werthen, A.G. Andersson, H.O. Björklund and S.T. Weiss. Current measurements using optical power, in Proc. Transmission and Distribution Conference, pages 213-218, 1996.

[6] S. Zadvornov and A. Sokolovsky. An Electro-Optic Hybrid Multifunctional Instrument for 3-Phase Current Measurements, in Proc. Conference on Instrumentation and Measurement Technology, 2008.

[7] H. Ramanitra, P. Chanclou, J. Etrillard, Y. Anma, H. Nakada and H. Ono. Optical access network using a self-latching variable splitter remotely powered through an optical fiber link. Optical Engineering, Vol. 46, No. 4, 2007.

[8] J.H. Lee, K.-M. Choi and C.-H. Lee. A Remotely Reconfigurable Remote Node for Next-Generation Access Networks. IEEE Photonic Technology Letters, Vol. 20, No. 11, pp. 915-917, 2008.

[9] A.P. Goutzoulis, J.M. Zomp, and A.H. Johnson. Development and Antenna Range Demonstration of an Eight-Element Optically Powered Directly Modulated Receive UHF Fiberoptic Manifold. IEEE Journal of Lightwave Technology, Vol. 14, No. 11, pp. 2499-2505, 1996.

[10] J. Lim, P.R. Jackson, B.E. Jones, K.F. Hale and Q.P. Yang. An intrinsically safe optically Powered hydraulic valve, in Proc. 7th International Conference on New Actuators, 2000, pages 216-219.

[11] D. Kuhn, E. Lo and T. Robbins. Powering Issues in an optical fiber customer access network, in Proc. 13th International Telecommunications Energy Conference, 1991, pages 51-58.

[12] S. Al-Chalabi, Optically powered telephone system over optical fiber with high service availability and low risk of investment in FTTH infrastructure. IEEE

Communications Magazine, Vol. 50, No. 8, pp. 102-109, August 2012.
[13] J.-G. Werthen. Powering Next Generation Networks by Laser Light over Fiber, in Proc. Optical Fiber communication/National Fiber Optic Engineers Conference, 2008, pages 1-3.
[14] M. Valentine. Power over Fiber Shines at Voltage Isolation. Power Electronics Technology, 2007.
[15] M. Matsuura and J. Sato. Power-over-fiber using double-clad fibers for radio-over-fiber systems, in Proc. 19th European Conference on Networks and Optical Communications - (NOC), Milano, Italy, June 2014, pages 126-131.
[16] T. Yasui, J. Ohwaki, M. Mino and T. Sakai. A Stable 2-W Supply Optical-Powering System, in Proc. 28th Photovoltaic Specialists Conference, 2000, pages 1614-1617.
[17] L.J. Cashdollar and K.P. Chen. Fiber Bragg Grating Flow Sensors Powered by In-Fiber Light. IEEE Sensors Journal, Vol. 5, No. 6, pp. 1327-1331, 2005.
[18] H. Miyakawa, E. Herawaty, M. Yoshimoto, Y. Tanaka, and T. Kurokawa. Power-Over-Optical Local Area Network Systems, in Proc. 3rd World Conference on Photovoltaic Energy Conversion, 2003, pages 2466-2469.
[19] R. Peña, C. Algora, I.R. Matias, and M. Loper-Amo. Fiberbased 205-mW (27% efficiency) power-delivery system for an all-fiber with optoelectronic sensor units. Applied optics, Vol. 38, No. 12, pages 2463-2466, 1999.
[20] T. Nango, T. Kawashima, J. Ohwaki and M. Tokuda. New Imitated Equipment with Optical Powering System for Evaluating Anechoic Chamber Characteristics, in Proc. International Symposium on Electromagnetic Compatibility, 2001, pages 274-279.
[21] G. Böttger *et al*. An Optically Powered Video Camera Link. IEEE Photonics Technology Letters, Vol. 20, No. 1, pp. 39-41, Jan 2008.
[22] J. Jeong, X. Jiangand and D. Culler. Design and analysis of micro-solar power systems for Wireless Sensor Networks, in Proc. of the 5th International Conference on Networked Sensing Systems (INSS 2008), 17-19 June 2008, pages 181-188
[23] P. Kamalinejad, C. Mahapatra, Z. Sheng, S. Mirabbasi, V.C.M. Leung and Y.L. Guanm. Wireless energy harvesting for the Internet of Things. IEEE Communication Magazine, Vol. 53, No. 6, pp. 102-108, June 2015.
[24] M. Gorlatova, J. Sarik, G. Grebla, M. Cong, I. Kymissis and G. Zussman. Movers and Shakers: Kinetic Energy Harvesting for the Internet of Things. IEEE Journal on Selected Areas in Communications, Vol. 33, No. 8, pp. 1624-1639, Aug. 2015.
[25] J. Wang *et al*. Power-over-fiber technique based sensing systems for internet of things, in Proc. 15th International Conference on Optical Communications and Network (ICOCN), Hangzhou, 2016, pages 1-3.
[26] H. Ujikawa, T. Yamada, K. I. Suzuki, A. Otaka, H. Nishiyama and N. Kato, Stand-Alone and Cooperative Deep Sleep for Battery-Driven Optical Network Unit, in IEEE Internet of Things Journal, Vol. 3, No. 4, pp. 494-502, Aug. 2016.
[27] T. Esram and P.L. Chapman. Comparison of Photovoltaic Array Maximum Power Point Tracking Techniques. IEEE Transactions on Energy Conversion, Vol. 22, No.2, pp. 439-449, June 2007.
[28] S. Lineykin, M. Averbukh and A. Kuperman. Five—parameter model of photovoltaic cell based on STC data and dimensionless, in Proc. IEEE 27th Convention of Electrical and Electronics Engineers in Israel, Eilat, Israel, 2012, pages 1-5.
[29] Analog Devices. Ultralow Power Energy Harvester PMUs with MPPT and Charge Management - AD5091-5092 datasheet, 2016.
[30] Analog Devices. ADP5091-2-EVALZ User Guide UG-927, 2016.
[31] P.H. Chou and C. Park. Energy-efficient platform designs for real-world wireless sensing applications, in Proc. IEEE ACM International Conference on Computer-Aided Design (ICCAD-2005), 6-10 November 2005, pages 913-920.
[32] C. Carvalho and N. Paulino. Indoor Light Energy Harvesting System for Wireless Sensing Applications. ISBN: 978-3-319-21616-4, Springer International Publishing, 2016.
[33] F. Simjee and P.H. Chou. Everlast: Long-life, Super-capacitor-operated Wireless Sensor Node, in Proc. 2006 International Symposium on Low Power Electronics and Design (ISLPED'06), 4-6 October 2006, pages 197-202.
[34] X. Jiang, J. Polastre and D. Culler. Perpetual environmentally powered sensor networks, in Proc. Fourth International Symposium on Information Processing in Sensor Networks (IPSN 2005), 15 April 2005, pages 463-468.
[35] EATON, PowerStor PB Family 5.0 volt cylindrical supercapacitors - Technical Data 4393, March 2015.
[36] EATON, PHB Supercapacitors Cylindrical pack - Technical Data 4402, June 2017.
[37] Wuhan Telecommunication Devices Co., RTXM167-522, Wuhan Telecommunication Devices Co. Ltd., 2012.